Bioorganic & Medicinal Chemistry Letters 19 (2009) 745–750

Contents lists available at ScienceDirect

Bioorganic & Medicinal Chemistry Letters

journal homepage: www.elsevier.com/locate/bmcl

5-Substituted pyrido[2,3-*d*]pyrimidine, an inhibitor against three receptor tyrosine kinases

Naparat Kammasud [a], Chantana Boonyarat [b], Kingkan Sanphanya [a], Maleeruk Utsintong [a], Satoshi Tsunoda [c], Hiroaki Sakurai [c], Ikuo Saiki [c], Isabelle André [d], David S. Grierson [d], Opa Vajragupta [a,*]

[a] *Department of Pharmaceutical Chemistry, Faculty of Pharmacy, Mahidol University, 447 Sri-Ayudhya Road, Bangkok 10400, Thailand*
[b] *Faculty of Pharmaceutical Sciences, Khon Kaen University, Khon Kaen 40002, Thailand*
[c] *Division of Pathogenic Biochemistry, Department of Bioscience, Institute of Natural Medicine, University of Toyama, Japan*
[d] *UMR 176 CNRS, Institut Curie, Section Recherche, Centre Universitaire, Bat.110-112, 91405 Orsay cedex, France*

ARTICLE INFO

Article history:
Received 15 August 2008
Revised 3 December 2008
Accepted 5 December 2008
Available online 10 December 2008

Keywords:
FGFR-1
FGFR-1 inhibitor
SU6668
5-Substituted indolin-2-one
Virtual screening
Docking
Binding mode
Anti-proliferation
Anti-angiogenesis

ABSTRACT

NP506, the 3-{2,4-dimethyl-5-[2-oxo-5-(*N*′-phenylhydrazinocarbonyl)-1,2-dihydro-indol-3-ylidenemethyl]-1*H*-pyrrol-3-yl}-propionic acid, was designed as FGF receptor 1 inhibitor by computational study and found to be more active against endothelial proliferation of HUVEC after the rhFGF-2 stimulation than SU6668 with minimum effective dose of 10 μM. NP506 inhibited the tyrosine phosphorylation in FGF, VEGF, and PDGF receptors and the activation of extracellular signal-regulated kinase (ERK), c-Jun-N-terminal-kinase (JNK) and AKT after the rhFGF-2 stimulation. The introduction of the phenyl hydrazide motif to the position 5 of the pyrido[2,3-*d*]pyrimidine scaffold led to the inhibitory effect in two signaling pathways: inhibition of AKT activation in the phosphatidyl inositol 3′-kinase (PI13K)/AKT signaling pathway and the inhibition of ERK and JNK activation in MAPK pathway.

We have previously reported the 6-substituted indolin-2-one, NP603,[1] as a novel inhibitor of FGFR. The binding affinity and selectivity for FGFR1 is attained through modification of the phenyl group attached to the 6-position of the pyrido[2,3-*d*]pyrimidine scaffold. In this report, we describe our efforts to explore the modification of the group attached to the 5-position of the pyrido[2,3-*d*]pyrimidine scaffold.

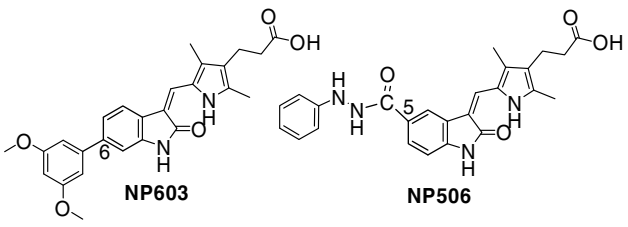

To study the role of structure on the inhibitory activity through FGFR1 binding which is essential for structure-based drug design, virtual screening was carried out. FGFR-1 target was constructed starting from X-ray structure of FGFR-1 in complex with SU4984 (PDB:1AGW[2]). The poorly ordered P-loop missing in 1AGW was rebuilt to give 1AGWRB, which was used as our protein model. The prepared FGFR1 template was validated by docking (FlexX, Tripos) with the three active inhibitors: SU5402, SU4984, and PD173074[1] for which the bound crystal structures are currently available. RMSD values when redocking with the 3 inhibitors were computed. In the docked poses with 1AGWRB, the three inhibitors were found to adopt the same configuration as in the crystal structures with RMSD less than 2 Å (0.69, 0.73, and 1.61 Å). Thus, 1AGWRB was a good model of FGFR1 protein template for virtual screening.

Virtual chemical libraries (A, B, C, and D) with variation of fragments substituted on the specified positions (Fig. 1) of oxindole were created. The diverse side chains corresponded to groups or fragments from an in-house database and from the 2003 version of MDL. Virtual combinatorial 2D-libraries were constructed by CombiLibMaker (Tripos), and all 3D structures were generated by Corina (Molecular Networks GmbH) and initially optimized with

* Corresponding author. Tel.: +66 2 6448677; fax: +66 2 6448695.
E-mail address: pyovj@mahidol.ac.th (O. Vajragupta).

0960-894X/$ - see front matter © 2008 Elsevier Ltd. All rights reserved.
doi:10.1016/j.bmcl.2008.12.023

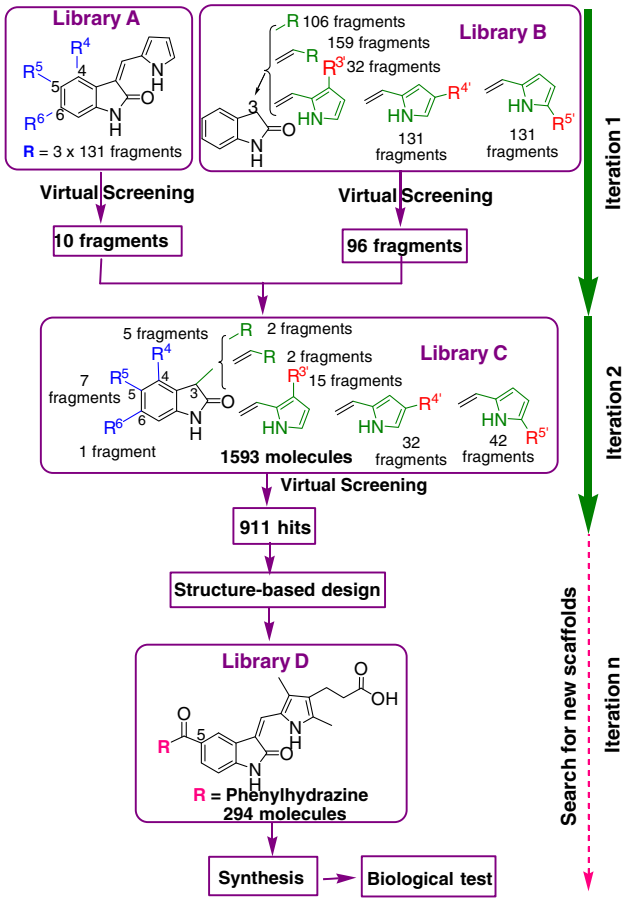

Figure 1. The procedure in library construction and virtual screening.

SYBYL7.0. All protons were added. Charges were assigned using the Gasteiger–Huckel method and ligand energies were minimized using the TRIPOS force field. During final preparations, Kollman charges were added, nonpolar hydrogens and lone pairs were merged, aromatic carbons identified, and lastly, the rigid root and rotatable bonds were defined.

Library A was prepared to study the role of substitutions at position 4, 5, and 6 on the oxindole ring while Library B was created in order to study the role of substituents at position 3 as well as to search for potential fragments. The oxindole at position 4, 5, and 6 of compounds in Library A were substituted with 131 fragments in each position. Library B, the oxindole, at position 3 were substituted with 106 fragments, 159 vinyl fragments, and 393 vinyl pyrrole fragments. The virtual screening process involved docking each molecule in the generated 3D-Libraries into the binding site of the FGFR1 tyrosine kinase model using a docking program, FlexX. All computational work was performed on a SGI Octane workstation equipped with the IRIX 6.5 operating system. The consensus-scoring module, consensus score (CScore) in SYBYL, version 7.0, made up of five scoring functions (G Score, D Score, PMF Score, Chem Score, and F Score), was used to estimate and rank the binding affinities. In iterative way, the fragments of the 25% top ranked structures from virtual screening were focused for further design (Fig. 1).

The results from virtual screening using Library A and B led to preparation of Library C. There are 393 molecules in Library A with 131 substituents which lead to 513 conformations in total. In Library B, there are 658 molecules with 396 substituents which lead to 1187 conformations in total. In the 25% top ranked structures from virtual screening of Library A (126 structures), there were 22 structures or hits with full consensus of 3, for example, hydrazine, hydrazide, phenyl urea, cinnamyl, cinnamoyl, and carbethoxy. Phenyl urea motif was in the 25% top ranked fragment but not as good as hydrazide motif whereas amide motif in position −5 was unable to form H-bonding with Glu562 and Ala564 leading to poor docking result. Ten fragments from the 22 hits were selected to be the fragments substituted at position 4, 5, or 6 of oxindole in Library C. In the 25% top ranked structures from virtual screening of Library B (295 structures), there were 153 hits with full consensus of 3. Ninety-six fragments from the 153 hits were selected to be the fragments substituted at position 3 of oxindole in Library C. Therefore, the selected fragments in Library C were ten fragments from Library A and ninety-six from Library B. In Library C, there are 1539 molecules with 106 substituents which lead to 7021 conformations in total. When focusing on the 25% top ranked structures from virtual screening in Library C, there were 911 hits with full consensus of 3. Compounds with hydrazide substituent at position 5 and the 2-carboxyethyl fragment in position −3 of the vinyl pyrrole ($R^{4'}$ in Fig. 1) were the top of the list.

From virtual screening results, the pharmacophore model of oxindole analogs binding at FGFR1 binding site was generated (Fig. 2). This model revealed the role of substituents at position 3, 4, 5, and 6 on the oxindole ring to binding in the ATP site. Among the oxindoles bearing substitutes at these positions, the modification at position 5 offers the best possibility to introduce a fragment bearing functional groups that could allow additional hydrogen bonding interactions with the Lys514 and/or a neighboring H_2O, and also reach the Asp641 for additional interactions. Similar interactions could be achieved from substitution at position 4; however position 5 remains the closest from Lys514 and Asp641 side chains.

Library D was constructed on the basis of the structural information obtained. In Library D, position 5 of oxindole was substituted with phenyl hydrazide fragments and position 3 was substituted with vinyl pyrrole fragment. The selected fragments in Library D corresponded to 294 fragments taken from commercial phenyl hydrazine fragments from MDL. NP506 and compounds **1**–**5** proved to be the most pertinent virtual hits in Library D. The binding energies of NP506 and compounds **1**–**5** with FGFR1 template were shown in Table 1. Among five compounds of interest, NP506 and compound **5** have the lowest docking energy.

The binding mode of NP506 with substitution of phenyl hydrazide motif at the 5-position of indolin-2-one was found to enhance the binding capacity via the hydrophobic interaction at the receptor pocket (Fig. 3).

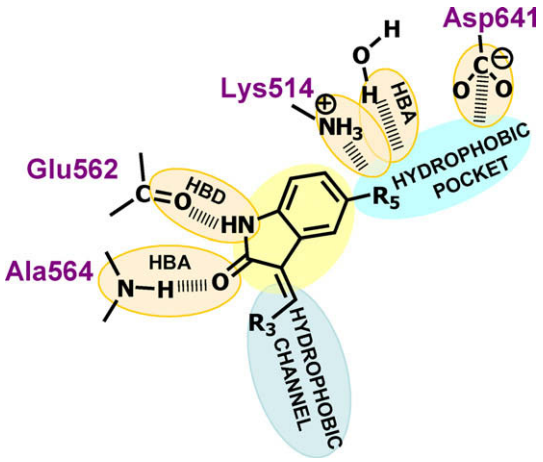

Figure 2. Model of the generated pharmacophore. HBA, hydrogen bond acceptor; HBD, hydrogen bond donor.

Table 1
Virtual hits and effect on the proliferation of HUVEC after the rhFGF-2 stimulation

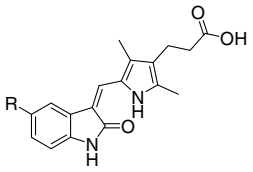

Compound	R	Docking energy (kcal/mol)	Min effective
SU6668	H	−10.2	10.0
1	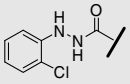	−11.7	50.0
NP506	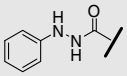	−13.0	10.0
3	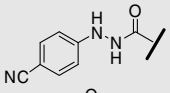	−12.7	>50.0
4	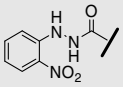	−11.6	50
5	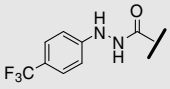	−13.1	50

The oxindone scaffold in NP506 structure makes three hydrogen bonds to the protein backbone of FGFR1: between N-1-oxindole and the carbonyl oxygen of Glu562, between carbonyl oxygen of the oxindole and the amide nitrogen of Ala564, and between N-1 of the pyrrole and the carbonyl oxygen of Ala564. These same two residues Glu562 and Ala564, located in the hinge region of FGFR1, are involved in hydrogen bonds to N-1 and N-6 in the adenine ring of ATP. The phenyl hydrazide substituted at position 5 locates into the hydrophobic pocket and forms two additional H-bonding interactions. The first is between carbonyl oxygen next to hydrazine and the NH_2 of Lys514, and the second involves the hydrazide NH (CON**H**NHPh) and carbonyl oxygen of Asp641, van der Waals contacts are made between the phenyl group and the side chains of Lys514, Ile545, Ala640, and Phe642 (Fig. 3b). The docking studies confirmed that the added substituent locates in the pocket and contributes to the hydrophobic type and hydrogen bonding interactions as expected.

As NP506 demonstrated good binding with FGFR1 in silico, it was synthesized along with related compounds (**1**, **3**–**5**) and SU6668 and evaluated in vitro for their kinase inhibition activity. The synthesis of NP506[4] was achieved by the synthetic Schemes 1 and 2.

The 5-substituted indolin-2-one **11** was prepared in six steps (260 mg, 38%), involving: reaction of dimethyl malonate (3 g, 23 mmol) and 1-fluoro-2-nitro-benzene (1.63 g, 11.6 mmol) to give 2-(2-nitro-phenyl)-malonic acid **6** (1.71 g, 66%), hydrolytic decarboxylation using 6 N aqueous hydrochloric acid to give (2-nitro-phenyl)-acetic acid **7** (1.4 g, 82%), reduction of nitro group using Pd-C as catalyst and cyclization to give indolin-2-one **8** (0.65 g, 70%), addition of chloroacetyl chloride (0.15 mol, 11.9 ml) to give **9**, followed by nucleophilic substitution of **9** using 2.5 N NaOH as nucleophile to give 2-oxo-2,3-dihydro-1H-indole-5-carboxylic acid **10** (5.05 g, 38%), and finally, coupling **10** with phenylhydrazine hydrochloride (368 mg, 2.56 mmol) to give **11** (260 mg, 38%) (Scheme 1). NP506 (84 mg, 77%) was obtained by condensation of 5-substituted indolin-2-one **11** (67 mg, 0.25 mmol) with pyrrole aldehyde **12** (49 mg, 0.25 mmol) which was prepared from methyl-5-(benzyloxycarbonyl) 2,4-dimethyl-3-pyrrole propionate as shown (Scheme 2). The structures of syn-

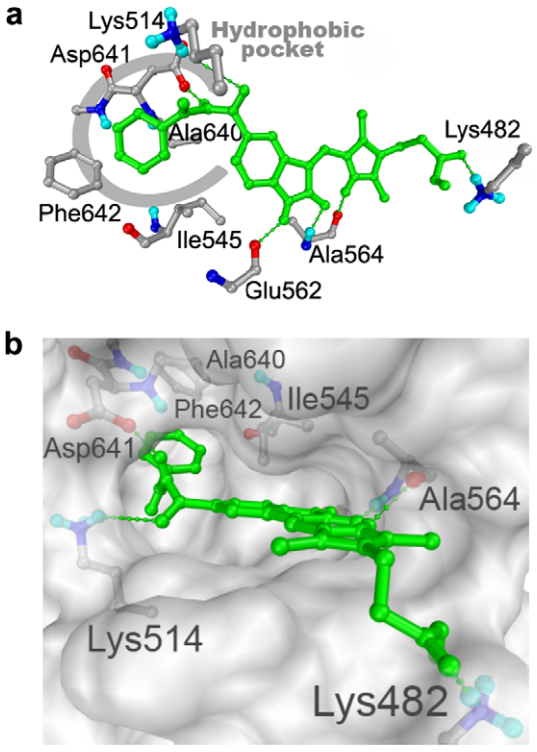

Figure 3. The binding modes of the FGFR1 kinase and NP506 (green) showing hydrogen bonds (green spheres) (a) and hydrophobic pocket (b).

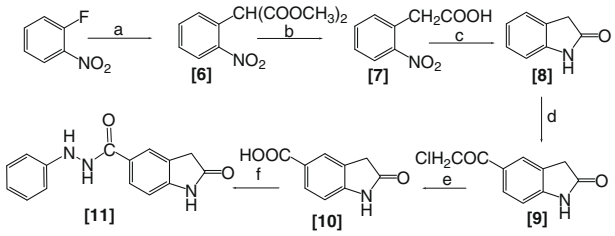

Scheme 1. Synthesis of 5-substituted indolinone. Reagents and conditions: (a) $CH_2(COOCH_3)_2$, NaH, THF, 100 °C, 3 h; (b) 6 N HClaq, overnight; (c) Pd/C, H_2, HOAc, rt, 4 h; (d) $AlCl_3$, CH_2Cl_2, 0 °C, $ClCH_2COCl$, 15 min, 45 °C, 2 h; (e) 1—pyridine 70–80 °C, 3 h; 2—2.5 N NaOH 70–80 °C, 3 h; 3—0.5 N HClaq, pH 2; (f) EDCI, HOBT, Et_3N, NH_2NHPh, DMF, rt, overnight.

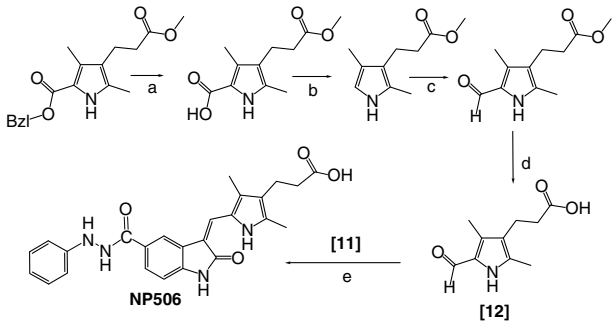

Scheme 2. Synthesis of NP506. Reagents and conditions: (a) Pd/C, H_2, EtOH, rt, 2 h; (b) TFA, reflux, 1 h; (c) TFA, trimethyl orthoformate, reflux, 1 h; (d) NaOHaq, reflux, 2 h; (e) 5-substituted indolin-2-one, piperidine **11**, EtOH, reflux, 3 h, then 2 N HClaq.

thesized compound were characterized by their melting points, FTIR, ^{1}H NMR, ^{13}C NMR, MS, and elemental analyses of C, H, and N. Spectral data (FTIR, NMR, and MS) were compatible with the assigned structures in all cases.

The in vitro inhibition of human FGFR1 kinase activity (expressed in insect cells) by NP506 was quantified by measuring the phosphorylation of the substrate biotinyl-βAβAβAAAEEYFFL-FAKKK and the HTRF detection method.[2] The IC_{50} against FGFR1 was found to be 0.1 μM, slightly better than NP603. FGF-2 is known to be one of the potent mitogens of vascular endothelial cells and to play an important role in the tumor-induced angiogenesis. Therefore, we determined the effect of NP506 and related compounds on the proliferation of human umbilical vein endothelial cells (HUVEC) after the recombinant human FGF-2 (rhFGF-2) treatment. All the tested compounds inhibited the rhFGF-2-induced cellular proliferation of HUVEC. NP506 has an inhibitory equipotent to SU6668. The minimum effective concentration of NP506 is 10 μM (Table 1). The minimum cytotoxic concentration of NP506 in the absence of rhFGF-2 was found to be 50 μM, which is five times greater than the minimum effective dose. Compounds **3**–**5** with the minimum effective anti-proliferation concentrations of 50 μM were considered inactive as the concentrations were close to their cytotoxic concentrations.

Selectivity of NP506 against other kinases such as VEGF,[5] PDGF,[6] and EGFR[7] were performed and the results are summarized in Table 2. NP503 exhibited good potency against 3 RTKs, FGFR1, VEGFR2, and PDGFRβ with different profile from SU6668 and NP603. The inhibition of PDGF signaling attributed to SU6668[6] oxindole scaffold while the inhibition of FGFR1 and VEGFR2 signaling were from the hydrophobic interaction of the phenylhydrazide motif at the receptor pocket in the same manner as 3,5-dimethoxyphenyl moiety in NP603 and PD173074 structures. Despite of two H-bonding with the same amino acid residues (Asp641 and Lys514), the phenylhydrazide motif in NP506 structure locates deeper in the pocket and confers the pi–pi interaction with Phe642 (Fig. 4a), leading to 5-fold increase in potency towards FGFR1.

When docking both compounds with VEGFR2 (PDB:2OH4),[8] the NP603 structure was found to align in opposite direction, the carboxylic acid in position −3 of the pyrrole locates in the receptor pocket instead of the 3,5-dimethoxyphenyl group. It is because VEGFR2 contains larger Cys917 and Val914 residues corresponding to Ala640 and Ile545 residues of FGFR1,[3] respectively, and consequently make the gate of the pocket too shallow to accommodate the bulky dimethoxyphenyl group (Fig. 4b). The increase in potency of NP506 to nM level against PDGFRβ was possibly due to additional interaction provided by cysteine residues of PDGFRβ corresponding to Ala640 and Ala564 of FGFR1. The effect of NP506 and NP603 in inhibiting the proliferation of HUVEC after rhFGF-2 treatment were found to be comparable which is due to the less cell accessibility of NP506, log*P* value of 2.292 versus 3.39 of NP603. Furthermore, NP506 showed moderate inhibition against EGFR.

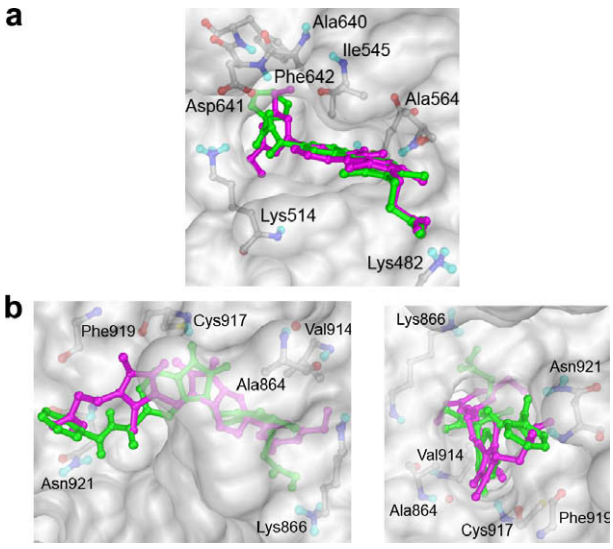

Figure 4. The binding modes of NP506 (green) and NP603 (magenta) with FGFR1 kinase (a) and VEGFR2 in different views (b).

The effect on the intracellular signaling in HUVEC after the rhFGF-2 treatment was further investigated by Western blot analysis. The serine/threonine kinase AKT or PKB, extracellular signal-regulated kinase (ERK) and c-Jun-N-terminal-kinase (JNK) play an important role in angiogenesis process for tumor growth and metastasis. Intracellular signaling cascade is the result of activation of AKT, ERK, and JNK which are the growth stimulating mediators. Phosphorylation of these mediators is necessary for tumor growth and metastasis. The growth factor induced activation of these mediators after the phosphorylation in FGF receptors. AKT has been implicated as anti-apoptoic mediator and its activation involved in endothelial cell survival and cell migration toward various matrix proteins.[9,10] Furthermore, resistance to radiation has been linked to the phosphatidyl inositol 3′-kinase (PI13K)/AKT signaling pathway.[11] It is increasingly evident that AKT is central to regulation of multiple pathways in endothelial cells and fibroblasts. While activation of ERK and JNK in mitogen-activated protein kinase (MAPK) pathway has been associated in growth factor induced cell proliferation and cell migration.[10,12,13] The result from Western blot analysis demonstrated that the NP506 treatment caused reduced phosphorylation of growth factor stimulating signaling mediators: AKT, ERK, and JNK in HUVEC cells. The level of

Table 2
Inhibition of tyrosine kinase activity and HUVEC proliferation after the rhFGF-2 stimulation

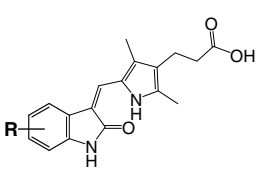

ID	R	Inhibition of tyrosine kinase activity (IC_{50}, μM)				Inhibition of cell proliferation (IC_{50}, μM)
		FGFR1	VEGFR2	PDGFRβ	EGFR	
SU6668	H	1.81	0.68	0.05	>100	>50
NP506	5-(CO-NHNHphenyl)	0.10	0.07	0.04	3.48	27.4
NP603	6-(3,5-diOCH_3phenyl)	0.52	0.93	0.78	>100	18.2

phosphorylated AKT and JNK (pAKT and pJNK) were inhibited completely by NP506 after FGF-2 stimulation while NP603 and SU6668 reduced the phosphorylation in the lesser extent. The decrease in phosphorylation of ERK by NP506 was more pronounced than SU6668 but in the lesser degree than NP603 (Fig. 5). Compared to SU6668, NP506 showed a stronger inhibitory effect of AKT, ERK, and JNK activation. The changing in position of the substitution from position 6 to position 5 resulted in inhibition of multiple signaling pathways implicated in cancer and cancer metastasis via angiogenesis. In addition to inhibition of MAPK signaling pathway, NP506 was able to inhibit (PI13K)/AKT signaling pathway.

These results indicate that NP506 has potent inhibitory activity on the FGF-2-induced tyrosine phosphorylation of 3 TK receptors, which resulted in the inhibition of ERK and JNK activation in MAPK pathway and AKT activation in (PI13K)/AKT pathway, leading to cellular proliferation in HUVEC.

To evaluate the effect of NP506 on angiogenesis, the HUVEC tube formation assay was performed in which the lengths of the capillary-like tubes formed were measured. NP506 suppressed HUVEC tubes formation in a dose dependent manner, in the presence of NP506, HUVECs formed incomplete and narrow tube-like structures (Fig. 6). In contrast, following stimulation with FGF-2, formation of elongated and robust tube-like structures was observed which were organized by a greater number of cells as compared to the control. Treatment with 1, 3, 10, and 25 μM of NP506 resulted in the inhibition of tube formation as compared with the control group. NP506 significantly inhibited tube formation in a concentration-dependent manner.

It was apparent that NP506, NP603, and SU6668 had comparable effect on angiogenesis according to the HUVEC tube formations assay. However, the profile of inhibition in signaling pathways are different. When comparing to SU6668, the effect of NP506 on angiogenesis appeared to be comparable despite the greater inhibition against tyrosine kinase and HUVEC proliferation after the rhFGF-2 stimulation. Hence, the contribution from other factors, that is, ADME might govern the same efficacy observed.

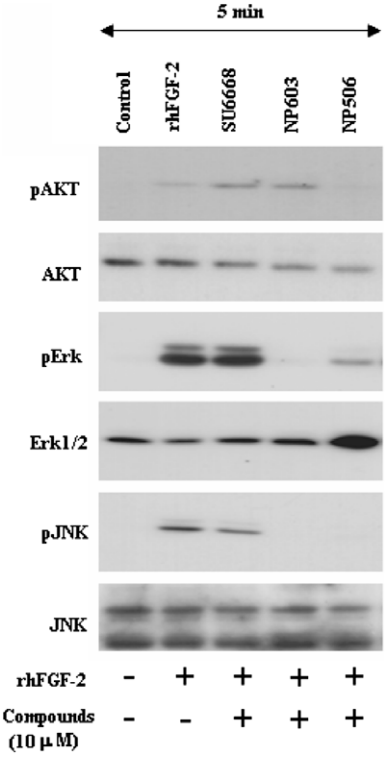

Figure 5. Effect on the intracellular signaling in HUVEC after the rhFGF-2 stimulation, Western blot of total proteins in HUVEC cell lysates with antibodies against JNK, phospho-specific JNK, ERK1/2, phospho-specific ERK, AKT, and phospho-specific AKT.

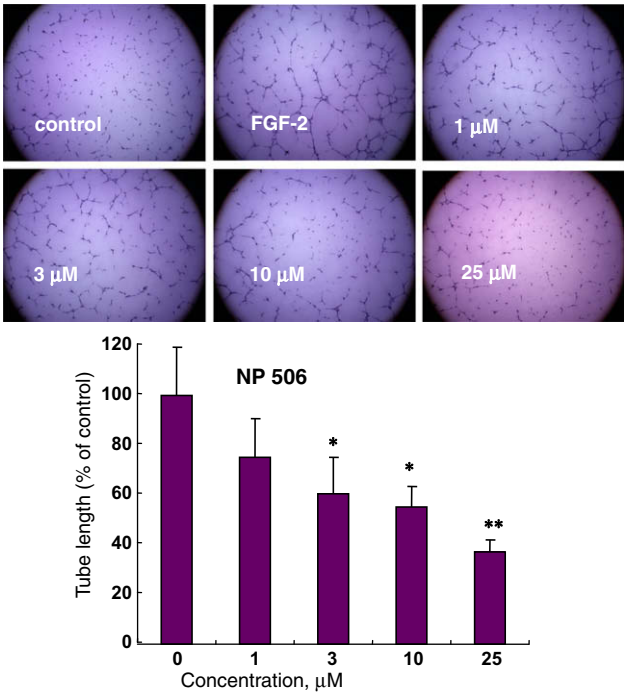

Figure 6. Effect of NP506 on the tube-like formations of HUVEC. HUVEC were seeded onto 96-well plates, which had been coated with 40 μl of Matrigel per well, in the presence of NP506. After a 4-h incubation period at 37 °C, the culture was fixed by glutaraldehyde, and the length of the tube-like formations was evaluated. Original magnification: 5×. A representative experiment is shown, with means + SD of four wells. $^{*}P < 0.05$, $^{**}P < 0.01$.

The introduction of the phenyl hydrazide motif at position 5 of the pyrido[2,3-*d*]pyrimidine scaffold has led to the inhibition of AKT activation in the phosphatidyl inositol 3′-kinase (PI13K)/AKT signaling pathway and the inhibition of ERK and JNK activation in MAPK pathway. The (PI13K)/AKT and MAPK pathway are the main signal transduction pathways implicated in cancer and cancer metastasis via angiogenesis.

Acknowledgments

This work was funded by the Royal Golden Jubilee Project, Thailand Research Fund, The Commission of Higher Education, Ministry of Education, Thailand and the 21st Century COE project from the Ministry of Education, Culture, Sports, Science and Technology, Japan.

References and notes

1. Kammasud, N.; Boonyarat, C.; Tsunoda, S.; Sakurai, H.; Saiki, I.; Grierson, D. S.; Vajragupta, O. *Bioorg. Med. Chem. Lett.* **2007**, *17*, 4812.
2. Mohammadi, M.; Froum, S.; Hamby, J. M.; Schroeder, M. C.; Panek, R. L.; Lu, G. H.; Dliseenkova, A. V.; Green, D.; Schlessinger, J.; Hubbard, S. R. *EMBO J.* **1998**, *17*, 5896.
3. Mohammadi, M.; McMahon, G.; Sun, L.; Tang, C.; Hirth, P.; Yeh, B. K.; Hubbard, S. R.; Schlessinger, J. *Science* **1997**, *276*, 955.
4. Melting point, IR, 1H, and ^{13}C NMR, mass, and elemental analysis (C, H, and N) determination. For NP506, 3-{2,4-dimethyl-5-[2-oxo-5-(*N*′-phenyl hydrazinocarbonyl)-1,2-dihydro-indol-3-ylidene-methyl]-1H-pyrrol-3-yl}-propionic acid as a mustard yellow solid: mp 232–234 °C; FTIR (KBr) (cm^{-1}): 3308 (N–H st.), 3101 (aromatic C–H st.), 2935 (aliphatic C–H st.), 1759, 1632 (C=O st.), 1547 (C=C st.), 1437 (bending C–H), 1146 (C–O st.); 1HNMR (300 MHz, DMSO-d_6) δ 13.35 (s, 1H, NH), 10.08 (s, 1H, NH), 8.29 (s, 1H, H4), 7.78 (s, 1H, NH), 7.77

(d, 2H, H2″, H6″), 7.70 (s, 1H, H6″), 7.67 (s, 1H, CH), 7.33 (t, 2H, H3″, H5″), 7.07 (d, 1H, H4″), 6.96 (d, 1H, H7), 2.61 (t, 2H, CH_2), 2.23 (t, 2H, CH_2), 1.47 (s, 6H, CH_3); ^{13}C NMR (300 MHz, DMSO-d_6); 174.63, 169.64, 165.88, 140.31, 139.45, 135.14, 130.72, 128.54, 127.68, 125.95, 125.83, 125.56, 124.04, 123.33, 123.23, 120.34, 117.23, 110.98, 108.72, 35.84, 20.04, 11.97, 9.52; MS *m*/*z* 443 [M−H], 444 [M]; elemental analysis CHN (67.74, 5.49, 12.53).

5. Itokawa, T.; Nokihara, H.; Nishioka, Y.; Sone, S.; Iwamoto, Y.; Yamada, Y.; Cherrington, J.; Mcmahon, G.; Shibuya, M.; Kuwano, M.; Ono, M. *Mol. Cancer Ther.* **2002**, *1*, 295.
6. Baxter, R. M.; Secrist, J. P.; Vaillancourt, R. R.; Kazlauskas, A. *J. Biol. Chem.* **1998**, *273*, 17050.
7. Weber, W.; Bertics, P. J.; Gill, G. N. *J. Biol. Chem.* **1984**, *259*, 14631.
8. Hasegawa, M.; Nishigaki, N.; Washio, Y.; Kano, K.; Harris, P. A.; Sato, H.; Mori, I.; West, R. I.; Shibahara, M.; Toyoda, H.; Wang, L.; Nolte, R. T.; Veal, J. M.; Cheung, M. *J. Med. Chem.* **2007**, *50*, 4453.
9. Somanath, P. R.; Razorenova, O. V.; Chen, J.; Byzova, T. V. *Cell Cycle* **2006**, *5*, 512.
10. Dailey, L.; Ambrosetti, D.; Mansukhani, A.; Basilico, C. *Cytokine Growth Factor Rev.* **2005**, *16*, 233.
11. McKenna, W. G.; Muschel, R. J. *Genes Chromosomes Cancer* **2003**, *38*, 330.
12. Eliceiri, B. P.; Klemke, R.; Strömblad, S.; Cheresh, D. A. *J. Cell Biol.* **1998**, *140*, 1255.
13. Yanagawa, T.; Funasaka, T.; Tsutsumi, S.; Watanabe, H.; Raz, A. *Endocr. Relat. Cancer* **2004**, *11*, 749.